Persistence of Strong Silica-Enriched Domains in the Earth's Lower Mantle

Maxim D. Ballmer[1,2], Christine Houser[1], John W. Hernlund[1], Renata M. Wentzcovitch[1,3,4] & Kei Hirose[1]

[1]*Earth-Life Science Institute, Tokyo Institute of Technology, Meguro, Tokyo, Japan.*

[2]*Institute of Geophysics, ETH Zurich, Zurich, Switzerland.*

[3]*Department of Applied Physics and Applied Mathematics, Columbia University, New York, USA.*

[4]*Department of Earth and Environmental Sciences, Columbia University, Lamont-Doherty Earth Observatory, Palisades NY, USA.*

The composition of the lower mantle – comprising 56% of Earth's volume – remains poorly constrained. Among the major elements, Mg/Si ratios ranging from ∼0.9–1.1, such as in rocky solar-system building blocks (or chondrites), to ∼1.2–1.3, such as in upper-mantle rocks (or pyrolite), have been proposed. Geophysical evidence for subducted lithosphere deep in the mantle has been interpreted in terms of efficient mixing and thus homogeneous Mg/Si across most of the mantle. However, previous models did not consider the effects of variable Mg/Si on the viscosity and mixing efficiency of lower-mantle rocks. Here, we use geodynamic models to show that large-scale heterogeneity with viscosity variations of ∼20×, such as due to the dominance of intrinsically strong (Mg,Fe)SiO_3−bridgmanite in low-Mg/Si domains, are sufficient to prevent efficient mantle mixing, even on large scales. Models predict that intrinsically strong domains stabilize degree-two mantle-convection pat-

terns, and coherently persist at depths of ∼1,000–2,200 km up to the present-day, separated by relatively narrow up-/downwelling conduits of pyrolitic material. The stable manifestation of such "bridgmanite-enriched ancient mantle structures" (BEAMS) may reconcile the geographical fixity of deep-rooted mantle-upwelling centers, and fundamental geophysical changes near 1,000 km depth (e.g. in terms of seismic-tomography patterns, radial viscosity increase, lateral deflections of rising plumes and sinking slabs). Moreover, these ancient structures may provide a reservoir to host primordial geochemical signatures.

State-of-the-art seismic-tomography models are difficult to reconcile with a mantle that is homogeneous (pyrolitic) on large length-scales. For example, most recently-subducted slabs flatten appearing to stagnate at either ∼660 km or ∼1,000 km depth[1]. Many mantle plumes are inferred to be deflected at similar depths[2,3]. In particular, deflections of mantle up-/downwellings in the uppermost lower mantle remain enigmatic. A viscosity increase near 1,000 km depth, consistent with geoid inversions, has been invoked to explain these observations[4,5]. However, there is no candidate phase transition to account for a sharp viscosity jump that could markedly affect mantle flow. Alternatively, compositional layering has been proposed[6], but the effects of coupled large-scale compositional and rheological heterogeneity on mantle dynamics remain poorly understood.

Composition-induced viscosity variations in the lower mantle

Lateral heterogeneity in lower-mantle composition can give rise to rheological contrasts. Heterogeneity involving SiO_2-enriched rocks has been put forward to balance the Earth's Si budget relative to the sun and chondrites, also given limitations to dissolve Si in the present-day

outer core[7]. SiO_2-enriched rocks with CI-chondritic Mg/Si of ∼0.9–1.1 should host ∼87-97% (Mg,Fe)SiO_3−bridgmanite (Br) and only ∼0-10% (Mg,Fe)O-ferropericlase (Fp), in addition to a minor amount of Ca-perovskite (∼3%). In contrast, pyrolitic rocks with Mg/Si ∼1.2–1.3) contain only ∼75-80% Br and up to ∼17-23% Fp in the lower mantle. As the viscosity of Br is estimated to be ∼1,000 times greater than that of Fp[8], and rheological models for rocks consisting of two phases[9] predict highly non-linear variations in rock viscosity as the modal abundance of the weak phase varies betweeen 0%–30% (Suppl. Figure S5), any SiO_2-enriched rocks (with relatively low Mg/Si and Fp content) are significantly more viscous than pyrolite in the lower mantle.

Intrinsically viscous rocks are thought to resist entrainment by mantle convection and processing at spreading centers[10]. However, the style of mantle convection in the presence of intense rheological contrasts due to large-scale compositional heterogeneity has not yet been quantitatively explored. We perform a suite of two-dimensional numerical experiments initially including a layer of intrinsically stronger, and modestly denser SiO_2-enriched rock in the lower mantle than the pyrolitic SiO_2-depleted material in the upper mantle (see methods). Model viscosity depends on temperature and composition, but composition-dependent rheology is limited to the lower mantle, where Fp+Br are the dominant stable phases (Suppl. Info.). We assume that SiO_2-enriched material (pyroxenite in the upper mantle) undergoes partial melting at $<$125 km depth to leave a SiO_2-poor pyrolitic residue[11]. The precise viscosity and density contrasts that may be relevant for the Earth's lower mantle are poorly constrained; therefore, we vary both parameters systematically.

We observe two regimes in our numerical experiments. In regime A, both materials are read-

ily mixed and the mantle becomes largely homogenized over time-scales shorter than the age of the Earth (Figure 1a-b). This regime occurs for relatively small viscosity contrasts between materials and is well-understood[12,13]. In regime B, we find instead that the intrinsically strong SiO_2-enriched material can avoid significant entrainment and mixing for model times greater than the age of the Earth (Figure 1c-f). A juxtaposition of both regimes is shown in Figure 1b-c as a comparison between the example case with moderate compositional viscosity and density contrasts (regime B), and reference case I with no such contrasts, but with a viscosity jump of factor λ=8 at 660 km depth (regime A). The viscosity jump is imposed to ensure comparable viscosity profiles and convective vigors between cases (Suppl. Info.).

A new regime of mantle convection

In the newly-described regime B, large-scale intrinsically strong SiO_2-enriched domains organize mantle-convection patterns. Initially, the upper-mantle pyrolitic material cools near the surface and soon sinks through the strong material in the lower mantle, thus forming relatively weak conduits. As the weaker material covers the core-mantle boundary and is heated, it becomes buoyant and rises upward through the strong layer to establish complementary upwelling conduits. Subsequently, the SiO_2-enriched material is encapsulated by the weaker pyrolite, which continues to circulate between the shallow and deepest mantle through the existing weak channels (Figure 1c-e). This encapsulation by weak material dramatically reduces stresses within strong domains. Therefore, strong domains – hereafter referred to as bridgmanite-enriched ancient mantle structures (BEAMS) – tend to avoid significant internal deformation, rather assuming slow coherent

rotation.

The weaker pyrolitic material slowly but progressively entrains SiO_2-enriched material as it circulates around BEAMS. Conduits thus contain an assemblage of SiO_2-poor and SiO_2-enriched materials, the latter of which would manifest as a pyroxenite-like mafic rock in the upper mantle. Note however that the SiO_2-poor pyrolitic material itself may consist of a fine-scale mixture of ultramafic to mafic rocks with compositions ranging from harzburgite to mid-ocean-ridge basalt (MORB). Our models also predict the ingestion of some weak plumes into BEAMS, particularly during early stages, which become stretched out into spiral shapes that persist as fossil fragments. Nevertheless, for sufficiently large viscosity contrast BEAMS remain largely coherent and stabilize lower mantle convection patterns over billions of years (Figure 1c,f). Little material crosses over from one conveyor circuit to another, giving rise to long-lived chemically-isolated domains. This tendency for isolation of convection cells suggests a possible mechanism for producing global-scale variations in MORB geochemistry[14], and preserving primordial reservoirs[15].

Persistence of BEAMS for 4.6 Gyrs or longer is predicted for respective density and viscosity contrasts of $\sim$0.4% and $>$20 (Figure 2). These contrasts are consistent with the effects of variable Mg/Si (or Br-content) on lower mantle density and viscosity (see Suppl. Info.). Density contrasts of $<$0.25% or $>$1% demand somewhat greater viscosity contrasts for long-term persistence, because any related rising or sinking (respectively) of BEAMS enhances viscous entrainment.

In the 3D spherical-shell geometry of Earth's mantle, BEAMS likely assume somewhat more complex shapes than suggested by our 2D-Cartesian models. 3D-BEAMS should assume

forms similar to donuts or rolls, minimizing internal deformation of high-viscosity domains (Suppl. Info.). Even though internal rotation of (donut-shaped) BEAMS may be difficult or even impossible in 3D, pyrolitic material would still circulate around BEAMS. Donut holes may accommodate upwelling centers (such as those beneath the Pacific and Africa), while downwelling curtains (such as those related to the subduction of Farallon and Tethys lithosphere) may occur between donuts/rolls. Such geometries are indeed suggested by maps of radially-averaged seismic velocities in the mid-mantle (Figure 3).

Comparison with geophysical observations

The BEAMS hypothesis can explain various seismic observations. We computed thermodynamic and thermoelastic properties for lower-mantle materials (see methods), and find that an average BEAMS mantle can match one-dimensional profiles such as PREM[16] (Suppl. Figure S2). Note however that one-dimensional seismic profiles alone are insufficient to discriminate between compositional models, particularly given current mineral-physics uncertainties[17–19] (Suppl. Info.). For example, a homogeneous pyrolitic mantle also provides an acceptable fit[20,21]. Nevertheless, the BEAMS model can further reconcile the fading of vertically-coherent fast anomalies (or subducted slabs) from tomography images in the mid-mantle[22–24] (Suppl. Info.). As BEAMS are intrinsically slightly faster than pyrolite due to higher Br contents, the seismic signal of slabs is predicted to fade relative to an average that is elevated by the presence of BEAMS (Suppl. Figure S7). Moreover, cluster analysis of shear-wave tomography models robustly requires three clusters at the inferred depths of BEAMS manifestation ($\sim$1,000–2,200 km)[25], while only two clusters

("slow" and "fast") are required in the deep lower mantle[24]. The geographical distribution of the third "neutral" cluster indeed agrees well with that of BEAMS inferred from Figure 3. Finally, radial coherence of large-scale seismic structure at depths >1,000 km is unrelated to upper-mantle seismic structure or plate-tectonic features[4,26], and thus points to an independent mechanism for large-scale heterogeneity at depth.

In particular, two key seismic observations can be better explained in the context of the BEAMS mantle than in that of a homogeneous-pyrolitic mantle. A regionally manifested compositional viscosity jump across BEAMS tops offers a simple explanation for the stagnation of some slabs at ~1,000 km depth[1], while other slabs readily sink through downwelling conduits at the same time[27]. Also, the location of stagnant slabs is consistent with the inferred geometry of BEAMS (Figure 3), and neutral clusters[25]. In turn, displacement of individual mantle plumes near 1,000 km depth[2,3] may be caused by circulation of mantle flow around BEAMS, and any related sub-horizontal "wind" in the upper mantle and transition zone.

The BEAMS hypothesis (Figure 4) further reconciles a range of other geophysical and geological constraints. For example, any mantle "wind" around BEAMS should be coupled to continental motions via cratonic keels, thereby supporting mountain building where it converges (i.e., above lower-mantle downwelling conduits such as across S-America and Asia)[28,29], and rifting where it diverges (i.e., above upwellings such as in E-Africa). Such coupling is reflected by quadrupole moments of plate-motion vectors, and quadrupole stability over ≥250 Myrs indicates that mantle-flow patterns persist through time[30], perhaps stabilized by BEAMS. Near the core-

mantle boundary, mantle circulation is predicted to converge around upwelling conduits in order to focus the generation and assent of plumes[3,31] beneath Africa and the south-central Pacific. These zones of convergence would also be the natural place for any (Fe-rich) dense mantle material to pile up, consistent with seismic images of large low shear-velocity provinces (LLSVP)[25,32–34] (see Figure 4). The long-term geographical fixity of these piles and plume-upwelling zones[31] again requires a mechanism for stabilization of mantle-flow patterns such as BEAMS. Otherwise, piles would readily respond to changes in mantle flow[35]. Accordingly, BEAMS may constrain the shapes of LLSVP-piles above the core-mantle boundary without requiring a delicate balance between viscous drag and gravitational forces[36]. Furthermore, probabilistic inversions of the geoid indicate a maximum of mantle viscosity (or "viscosity hill") in the mid-mantle[4]. While a viscosity hill is not uniquely required by the data within uncertainties, it would indeed naturally arise from the manifestation of intrinsically strong BEAMS at about 1,000–2,200 km depth. We stress that the presence of BEAMS is not the only possible cause for any of these observations, but can provide a straightforward unified explanation, and thus should be thoroughly tested.

Future quantitative tests of the BEAMS hypothesis should involve systematic studies of seismic reflections and seismic anisotropy in the lower mantle. Our models predict that underside as well as out-of-plane reflections should preferentially occur near BEAMS margins with dominantly positive polarities. Whereas reflections and conversions of seismic waves have indeed been commonly observed in the uppermost lower mantle, e.g. near the expected tops of BEAMS[6,37], a systematic study that could map any large-scale compositional heterogeneity is lacking. The predicted circulation around BEAMS further implies vertically-fast seismic anisotropy within up-

and downwelling conduits (due to lattice-preferred[38] or shape-preferred [9] orientation), as well as horizontally-fast anisotropy above and below BEAMS. The latter prediction is consistent with observations of anisotropy beneath the Tonga slab that stagnates at ∼1,000 km depth[1,39,40], but more detailed regional studies of mid-mantle anisotropy are needed.

Geochemical implications

The geochemical implications of the BEAMS hypothesis depend on the origin scenario. An initial global lower-mantle SiO_2-enrichment compatible with our model starting conditions could arise due to (1) incomplete equilibration of the proto-mantle during multi-stage core formation[41], (2) fractionation during magma-ocean crystallization[42], and/or (3) continental extraction that leaves the shallow pyrolitic domain as a "depleted MORB mantle" residue. If BEAMS formed within ∼100 Myrs after Earth's formation (scenarios 1 and/or 2), then they would be viable candidates for hosting primordial noble-gas reservoirs[43,44] as well as primordial ^{182}W[45], because BEAMS material is never processed through the shallow upper mantle. Note that at least in scenario (2) BEAMS would moreover be better candidates to host primordial geochemical signatures (such as e.g. FOZO[46]) than LLSVPs, because they would be relatively depleted in incompatible elements[47]. The predicted dynamical behavior of mostly stable BEAMS with gradual entrainment along margins provides the conditions for primordial reservoirs to be preserved in a vigorously convecting mantle, but also be sampled by hotspot lavas at the same time, along with recycled geochemical components[46–48]. In contrast to small-scale blobs that have previously been invoked to host primitive material[10,49], BEAMS can provide a large-scale coherent primordial reservoir of up

to 10%$\sim$15% of the mantle's mass (Suppl. Info.). Such large-scale heterogeneity may balance Earth's bulk composition, e.g. bringing it closer to solar-chondritic Mg/Si-ratios.

Figure caption references[50,51]

Methods

We here describe the methodology of geodynamic models, as well as of the computation of thermodynamic and thermoelastic properties. For figures and more detailed discussion, we refer the reader to the main text as well as the Suppl. Information.

Numerical mantle-convection models. In order to study thermochemical convection of the mantle, we used an advanced version of mantle-convection code CitcomCU[52,53]. On the finite-element mesh, we solved the conservation equations of mass, momentum and energy applying the Boussinesq approximation. Composition is tracked using passive particles (or "tracers"). The model box is 2,900 km deep and 17,400 km wide. The vertical resolution of the model varies between 16.5 km and $\sim$18.7 km due to mesh refinement in the upper mantle. Horizontal resolution is 17 km. Initial conditions involve a difference in composition between the upper and lower mantles. In the upper mantle, tracer values are set to a compositional index of zero, representing SiO_2-poor mantle material similar to pyrolite. In the lower mantle, tracer values are randomly set to a compositional index of 0.95 ± 0.05, representing (Mg,Fe)SiO_3-rich (or SiO_2-rich) mantle material (Suppl. Figure S1). Random compositional noise of ± 0.05 is added in the lower mantle in order to seed small non-diffusive perturbations that help to break the strong deep layer. Initial potential temperatures are 2,000 °C in the mid-mantle with thermal boundary layers at the top and bottom (calculated from 80-Myr halfspace cooling profiles), plus a small random thermal noise. Boundary conditions involve potential temperatures of T_{surf} = 0 °C and T_{CMB} = 3000 °C at the top and bottom, respectively, as well as free-slip velocity conditions on all sides. The applied T_{CMB} is well in the range of estimates[54,55] (note that the adiabat needs to be added to T_{CMB} for proper comparison

with estimates of "real" CMB temperature).

Distinct physical properties are assigned to the two materials. SiO_2-rich material is denser (by $\Delta\rho$) and stiffer (by a factor of Φ) than peridotitic material. While the density difference is applied everywhere in the mantle, the viscosity contrast is only applied in the lower mantle. This parameterization is motivated by the limitation of the stability of Br and Fp (i.e., to lower-mantle pressures), the presence of which in variable proportions between the materials is envisioned to account for the viscosity contrast (see Suppl. Info. and main text). Additionally, we prescribed that all "SiO_2-enriched" tracers, which enter the shallowest part of the mantle (i.e. at depths $<$125 km), are immediately turned into "pyrolitic tracers" (i.e., tracer values are set to zero), assuming that SiO_2-rich material undergoes melting to become relatively enriched in MgO. Such a depth of melting for (Mg,Fe)SiO_3-rich rocks is supported experimentally[11].

In our geodynamic models, we applied a Newtonian rheology with moderate temperature dependence of viscosity, and no depth dependence. Viscosity varies by six orders of magnitude over the full thermal range of $T_{CMB} - T_{surf}$, but a cutoff is applied at four orders of magnitude in the stiff thermal boundary layer at the top (see Figure 1e in the main text) in order to ensure numerical stability. Depth-dependency of thermal expansivity is accounted for (according to ref. [6]). For all other parameters, see Suppl. Table 2.

In order to systematically study the effects of intrinsic variations in density and viscosity on mantle flow, we performed a systematic parameter search by varying $\Delta\rho$ and Φ. For a list of all cases, see Suppl. Table 3. $\Delta\rho$ is varied in the range of 0 and 65 kg/m^3 (i.e., 0%-1.444%), and Φ

in the range of 3.136 to 249.1. We explored this parameter space by running 26 simulations with no imposed viscosity jump at 660 km depth (i.e., λ = 1). A regionally variable viscosity jump at 660 km depth self-consistently arises from our treatment of compositional rheology: as compositional rheology is restricted to the lower mantle (see above), a viscosity jump arises wherever compositional index >0. We also explored three reference cases $\lambda > 1$. For a detailed description and discussion of these reference cases, as well as for the post-processing and analysis of numerical-model predictions, see Suppl. Information.

Computation of seismic velocities and densities. One-dimensional seismic-velocity and density profiles are calculated for comparison with PREM[16] (Suppl. Figure S2). For this calculation, we used thermodynamic and thermoelastic properties of $Mg_{1-x}Fe_xSiO_3$ bridgmanite (Br) and $Mg_{1-y}Fe_yO$ ferropericlase (Fp) as previously computed by refs. [56] and [57,58], respectively, for iron numbers $x = 0$ and $x = 0.125$, as well as $y = 0$ and $y = 0.1875$. For all other x and y values, physical properties have been linearly interpolated. For $CaSiO_3$ perovskite, thermoelastic properties calculated by Kawai and Tsuchiya[59] were reproduced within the Mie-Debye-Grüneisen formalism as outlined by Stixrude and Lithgow-Bertelloni[60] using density functional theory (DFT) within the local density approximation (LDA) that is augmented by the Hubbard U (LDA+U). These thermoelastic properties were calculated self-consistently for Fe, Si, and O along with psuedopotentials for Mg. Details of the LDA and LDA+U calculations are reported in refs. [56–59].

We considered mixtures in the SiO_2–MgO–CaO–FeO oxide space for aggregates with harzburgitic[61], pyrolytic[62], and perovskititic (i.e. pure Br) compositions[63]. For the specific oxide compositions of these aggregates, see Suppl. Table 1. Perovskititic compositions have been computed by in-

crementally removing MgO from pyrolite. Note that calculations do not incorporate the effects of Al_2O_3. In the adjusted compositions, the number of moles of Al_2O_3 have been equally distributed between MgO and SiO_2. The iron partitioning coefficient, K_D, between Fp and Br was kept constant at 0.5[64]. Density and seismic-velocity profiles for these end-member compositions are shown in Supplementary Figure S3.

To compute these profiles, we used the self-consistent geotherms shown in Supplementary Figure S4. Moduli and densities for each of the minerals were interpolated along the calculated geotherms; physical properties of mineral assemblages have been obtained using the Voigt-Reuss-Hill (VRH) average. To calculate the adiabatic geotherms, the following equation has been integrated to solve for T(P)[65], where the aggregate quantities are the molar volume, the thermal expansion coefficient, and the isobaric specific heat of aggregates: $(\partial T/\partial P)_S = \alpha_{agg} V_{agg} T / C_{p_{agg}}$. In these calculations, the temperature at the top of the lower mantle (23 GPa) is anchored at 1873 K, as constrained by the post-spinel transition[66].

Finally, to compute density and seismic-velocity profiles for the BEAMS mantle, we used an idealized average composition of the lower mantle. Inspired by our numerical-model predictions, we assumed that 50% of the lower mantle is composed of perovskitite (i.e. pure Br), and 25% is composed of each cold and warm harzburgite (downwellings and upwellings, respectively). The relevant adiabats of these components are shown in Supplementary Figure S4.

Method references. Reference numbers 51-65 (see reference list below).

References

1. Fukao, Y. & Obayashi, M. Subducted slabs stagnant above, penetrating through, and trapped below the 660 km discontinuity. *J. Geophys. Res.* **118**, 5920–5938 (2013).

2. Rickers, F., Fichtner, A. & Trampert, J. The Iceland–Jan Mayen plume system and its impact on mantle dynamics in the North Atlantic region: Evidence from full-waveform inversion. *Earth and Planetary Science Letters* **367**, 39–51 (2013).

3. French, S. W. & Romanowicz, B. Broad plumes rooted at the base of the Earth's mantle beneath major hotspots. *Nature* **525**, 95–99 (2015).

4. Rudolph, M., Lekic, V. & Lithgow-Bertelloni, C. Viscosity jump in Earth's mid-mantle. *Science* **350**, 1349–1352 (2015).

5. Marquardt, H. & Miyagi, L. Slab stagnation in the shallow lower mantle linked to an increase in mantle viscosity. *Nature Geoscience* **8**, 311–314 (2015).

6. Ballmer, M. D., Schmerr, N. C., Nakagawa, T. & Ritsema, J. Compositional mantle layering revealed by slab stagnation at ∼1000-km depth. *Science Advances* **1**, doi:10.1126/sciadv.1500815 (2015).

7. Badro, J., Côté, A. S. & Brodholt, J. P. A seismologically consistent compositional model of Earth's core. *Proceedings of the National Academy of Sciences* **111**, 7542–7545 (2014).

8. Yamazaki, D. & Karato, S.-I. Some mineral physics constraints on the rheology and geothermal structure of Earth's lower mantle. *Amer. Mineralogist* **86**, 385–391 (2001).

9. Girard, J., Amulele, G., Farla, R., Mohiuddin, A. & Karato, S.-I. Shear deformation of bridgmanite and magnesiowüstite aggregates at lower mantle conditions. *Science* **351**, 144–147 (2016).

10. Manga, M. Low-viscosity mantle blobs are sampled preferentially at regions of surface divergence and stirred rapidly into the mantle. *Physics of the Earth and Planetary Interiors* **180**, 104–107 (2010).

11. Pertermann, M. & Hirschmann, M. M. Partial melting experiments on a MORB-like pyroxenite between 2 and 3 GPa: Constraints on the presence of pyroxenite in basalt source regions from solidus location and melting rate. *Journal of Geophysical Research: Solid Earth* **108**, 2125, doi:10.1029/2000JB000118 (2003).

12. Kellogg, L. Chaotic mixing in the Earth's mantle. In Dmowska, R. & Saltzman, B. (eds.) *Advances in Geophysics*, vol. 34, 1–33 (Academic Press, 1993).

13. Coltice, N. & Ricard, Y. Geochemical observations and one layer mantle convection. *Earth Planet. Sci. Letter.* **74**, 125–137 (1999).

14. Dupré, B. & Allègre, C. J. Pb-Sr isotope variation in Indian Ocean basalts and mixing phenomena. *Nature* **303**, 142–146 (1983).

15. Schubert, G. & Spohn, T. Two-layer mantle convection and the depletion of radioactive elements in the lower mantle. *Geophys. Res. Lett.* **8**, 951–954 (1981).

16. Dziewonski, A. & Anderson, D. Preliminary reference Earth model. *Phys. Earth Planet. Inter.* **25**, 297–356 (1981).

17. Murakami, M., Ohishi, Y., Hirao, N. & Hirose, K. A perovskitic lower mantle inferred from high–pressure, high–temperature sound velocity data. *Nature* **485**, 90–95 (2012).

18. Ismailova, L. *et al.* Stability of Fe, Al-bearing bridgmanite in the lower mantle and synthesis of pure Fe-bridgmanite. *Science Advances* **2**, doi:10.1126/sciadv.1600427 (2016).

19. Matas, J., Bass, J., Ricard, Y., Mattern, E. & Bukowinski, M. On the bulk composition of the lower mantle: predictions and limitations from generalized inversion of radial seismic profiles. *Geophysical Journal International* **170**, 764–780 (2007).

20. Wang, X., Tsuchiya, T. & Hase, A. Computational support for a pyrolitic lower mantle containing ferric iron. *Nature Geoscience* **8**, 556–559 (2015).

21. Hyung, E., Huang, S., Petaev, M. I. & Jacobsen, S. B. Is the mantle chemically stratified? Insights from sound velocity modeling and isotope evolution of an early magma ocean. *Earth and Planetary Science Letters* **440**, 158–168 (2016).

22. Hernlund, J. & Houser, C. On the distribution of seismic velocities in Earth's deep mantle. *Earth Planet. Sci. Lett.* **265**, 423–437 (2008).

23. Houser, C. & Williams, Q. The relative wavelengths of fast and slow velocity anomalies in the lower mantle: Contrary to the expectations of dynamics? *Phys. Earth Planet. Int.* **176**, 187–197 (2009).

24. Lekic, V., Cottaar, S., Dziewonski, A. & Romanowicz, B. Cluster analysis of global lower mantle tomography: A new class of structure and implications for chemical heterogeneity. *Earth Planet. Sci. Lett.* **357-358**, 68–77 (2012).

25. Cottaar, S. & Lekic, V. Morphology of seismically slow lower-mantle structures. *Geophysical Journal International* **207**, 1122–1136 (2016).

26. Dziewonski, A., Lekic, V. & Romanowicz, B. Mantle anchor structure: An argument for bottom up tectonics. *Earth and Planetary Science Letters* **299**, 69–79 (2010).

27. Van Der Meer, D. G., Spakman, W., Van Hinsbergen, D. J., Amaru, M. L. & Torsvik, T. H. Towards absolute plate motions constrained by lower-mantle slab remnants. *Nature Geoscience* **3**, 36–40 (2010).

28. Becker, T. & Faccenna, C. Mantle conveyor beneath the Tethyan collisional belt. *Earth and Planetary Science Letters* **310**, 453–461 (2011).

29. Faccenna, C., Becker, T., Conrad, C. & Husson, L. Mountain building and mantle dynamics. *Tectonics* **32**, 80–93 (2013).

30. Conrad, C. P., Steinberger, B. & Torsvik, T. H. Stability of active mantle upwelling revealed by net characteristics of plate tectonics. *Nature* **498**, 479–482 (2013).

31. Torsvik, T. H., Burke, K., Steinberger, B., Webb, S. J. & Ashwal, L. D. Diamonds sampled by plumes from the core-mantle boundary. *Nature* **466**, 352–355 (2010).

32. Garnero, E. J. & McNamara, A. K. Structure and dynamics of Earth's lower mantle. *Science* **320**, 626–628 (2008).

33. Deschamps, F., Cobden, L. & Tackley, P. J. The primitive nature of large low shear-wave velocity provinces. *Earth and Planetary Science Letters* **349**, 198–208 (2012).

34. Ballmer, M. D., Schumacher, L., Lekic, V., Thomas, C. & Ito, G. Compositional layering within the large low shear-wave velocity provinces in the lower mantle. *Geochemistry, Geophysics, Geosystems* **17**, doi:10.1002/2016GC006605 (2016).

35. McNamara, A. K. & Zhong, S. Thermochemical structures beneath Africa and the Pacific Ocean. *Nature* **437**, 1136–1139 (2005).

36. Tan, E. & Gurnis, M. Compressible thermochemical convection and application to lower mantle structures. *Journal of Geophysical Research: Solid Earth* **112**, doi:10.1029/2006JB004505 (2007).

37. Jenkins, J., Deuss, A. & Cottaar, S. Converted phases from sharp 1000 km depth mid-mantle heterogeneity beneath western europe. *Earth and Planetary Science Letters* **459**, 196–207 (2016).

38. Tsujino, N. *et al.* Mantle dynamics inferred from the crystallographic preferred orientation of bridgmanite. *Nature* **539**, 81–84 (2016).

39. Wookey, J. & Kendall, J.-M. Evidence of midmantle anisotropy from shear wave splitting and the influence of shear-coupled P waves. *Journal of Geophysical Research: Solid Earth* **109**, doi:10.1029/2003JB002871 (2004).

40. Chang, S.-J., Ferreira, A. M. & Faccenda, M. Upper-and mid-mantle interaction between the Samoan plume and the Tonga-Kermadec slabs. *Nature communications* **7**, doi:10.1038/ncomms10799 (2016).

41. Kaminski, E. & Javoy, M. A two-stage scenario for the formation of the Earth's mantle and core. *Earth and Planetary Science Letters* **365**, 97–107 (2013).

42. Elkins-Tanton, L. Linked magma ocean solidification and atmospheric growth for Earth and Mars. *Earth and Planetary Science Letters* **271**, 181–191 (2008).

43. Mukhopadhyay, S. Early differentiation and volatile accretion recorded in deep-mantle neon and xenon. *Nature* **486**, 101–104 (2012).

44. Caracausi, A., Avice, G., Burnard, P. G., Füri, E. & Marty, B. Chondritic xenon in the Earth's mantle. *Nature* **533**, 82–85 (2016).

45. Rizo, H. *et al.* Preservation of Earth-forming events in the tungsten isotopic composition of modern flood basalts. *Science* **352**, 809–812 (2016).

46. Hart, S., Hauri, E. *et al.* Mantle plumes and entrainment: Isotopic evidence. *Science* **256**, 517–520 (1992).

47. White, W. Isotopes, DUPAL, LLSVPs, and Anekantavada. *Chemical Geology* **419**, 10–28 (2015).

48. Garapić, G., Mallik, A., Dasgupta, R. & Jackson, M. G. Oceanic lavas sampling the high-3He/4He mantle reservoir: Primitive, depleted, or re-enriched? *American Mineralogist* **100**, 2066–2081 (2015).

49. Becker, T. W., Kellogg, J. B. & O'Connell, R. J. Thermal constraints on the survival of primitive blobs in the lower mantle. *Earth and Planetary Science Letters* **171**, 351–365 (1999).

50. Parmentier, E. M., Turcotte, D. L. & Torrance, K. E. Studies of finite amplitude non-Newtonian thermal convection with application to convection in the Earth's mantle. *Journal of Geophysical Research* **81**, 1839–1846 (1976).

51. Houser, C., Masters, G., Shearer, P. & Laske, G. Shear and compressional velocity models of the mantle from cluster analysis of long-period waveforms. *Geophys. J. Int.* **174**, 195–212 (2008).

52. Moresi, L., Zhong, S. & Gurnis, M. The accuracy of finite element solutions of Stokes's flow with strongly varying viscosity. *Physics of the Earth and Planetary Interiors* **97**, 83–94 (1996).

53. Ballmer, M., Van Hunen, J., Ito, G., Bianco, T. & Tackley, P. Intraplate volcanism with complex age-distance patterns: A case for small-scale sublithospheric convection. *Geochemistry, Geophysics, Geosystems* **10**, doi:10.1029/2009GC002386 (2009).

54. Lay, T., Hernlund, J. & Buffett, B. A. Core–mantle boundary heat flow. *Nature Geoscience* **1**, 25–32 (2008).

55. Nomura, R. *et al.* Low core-mantle boundary temperature inferred from the solidus of pyrolite. *Science* **343**, 522–525 (2014).

56. Shukla, G. *et al.* Thermoelasticity of Fe^{2+}-bearing bridgmanite. *Geophys. Res. Lett.* **42**, 1741–1749 (2015).

57. Wu, Z., Justo, J., da Silva, C., de Gironcoli, S. & Wentzcovitch, R. M. Anomalous thermodynamic properties in ferropericlase throughout its spin crossover transition. *Physical Review B* **80**, doi:10.1103/PhysRevB.80.014409 (2009).

58. Wu, Z., Justo, J. & Wentzcovitch, R. Elastic anomalies in a spin-crossover system: Ferropericlase at lower mantle conditions. *Phys. Rev. Lett.* **110**, doi:10.1103/PhysRevLett.110.228501 (2013).

59. Kawai, K. & Tsuchiya, T. P-V-T equation of state of cubic $CaSiO_3$ perovskite from first-principles computation. *J. Geophys. Res.* **119**, 2801–2809 (2014).

60. Stixrude, L. & Lithgow-Bertelloni, C. Thermodynamics of mantle minerals -I. Physical properties. *Geophys. J. Int.* **162**, 610–632 (2005).

61. Baker, M. & Beckett, J. The origin of abyssal peridotites: A reinterpretation of constraints based on primary bulk compositions. *Earth Planet. Sci. Lett.* **171**, 49–61 (1999).

62. McDonough, W. & Sun, S. The composition of the Earth. *Chem. Geo.* **120**, 223–253 (1995).

63. Williams, Q. & Knittle, E. The uncertain major element bulk composition of Earth's mantle. *Earth's Deep Mantle: Structure, Composition, and Evolution. Geophysical Monograph Series* **160**, 187–199 (2005).

64. Irifune, T. *et al.* Iron partitioning and density changes of pyrolite in Earth's lower mantle. *Science* **327**, 193–195 (2010).

65. Valencia-Dardona, J., Shukla, G., Wu., Z., Yuen, D. & Wentzcovitch, R. Impact of spin crossover in ferropericlase on the lower mantle adiabat. *Geophys. Res. Lett.* in review (2016).

66. Irifune, T. *et al.* The postspinel phase boundary in Mg_2SiO_4 determined by in situ X-ray diffraction. *Science* **279**, 1698–1700 (1998).

Acknowledgements. The authors thank Frédéric Deschamps and an anonymous reviewer for their comments that helped to improve the manuscript. They are further grateful to Adam Dziewonski for discussions on the seismic structure and dynamics of the mantle. Calculations have been performed on akua, the in-house cluster of the Department of Geology&Geophysics, Univ. Hawaii. The numerical tools used here, as well as model input and output, are available upon request. M.D.B., C.H., J.W.H., and K.H. were supported by the WPI-funded Earth-Life Science Institute at Tokyo Institute of Technology. C.H., J.W.H., and K.H. received further support through MEXT KAKENHI grant numbers 15H05832 and 16H06285. R.M.W. was funded through NSF grants EAR-1319361 and EAR1348066.

Author Contributions. M.D.B., C.H., and J.W.H. wrote the manuscript and composed the figures. M.D.B. performed and analyzed geodynamic models. C.H. and R.M.W. computed seismic velocities in the lower mantle. J.W.H. and K.H. analyzed the influence of composition on density and viscosity. All authors contributed to the BEAMS hypothesis, and the design of the study.

Competing Financial Interests. The authors declare that they have no competing financial interests.

Corresponding authors. Correspondence and requests for materials should be addressed to M.D.B..

Figure 1 Numerical-model results for (A-B) reference case I, and the (C-F) example case after (A-E) 4.6 Gyrs and (F) 10 Gyrs model time. (B,C,F) Snapshots of composition with isotherms (spaced 450 K). (A,D) Snapshots of temperature with compositional contour that marks small-scale heterogeneity in (A), and large-scale BEAMS in (D). This difference in mantle-mixing efficiency between cases highlights the role of compositional rheology, given that both cases have similar Nusselt numbers *Nu* (Suppl. Table S3), i.e. a criterion for convective vigor[50]). (E) Snapshot of viscosity shows that BEAMS are more viscous than upwelling and downwelling conduits. Also see Suppl. Movies S1-S4.

Figure 2 Summary of numerical-model results. Regime map of all cases (Suppl. Table 3) shows that compositional-viscosity contrasts of $\sim$1.5 orders of magnitude and small-to-moderate compositional density contrasts are required for long-term persistence of SiO_2-enriched material (blue squares). This conclusion is independent of whether all cases, or the subset of cases with $10 \leq Nu \leq 11$ (yellow highlighted) are considered. In reference cases I/II and III (circles), a global viscosity jump at 660 km depth of factor λ=8 and λ=2.5, respectively, is imposed to ensure that *Nu* is comparable to *Nu* of the example case (Figure 1c-f), which is marked by a white cross.

Figure 3 Map with possible distributions of BEAMS in the Earth's lower mantle. Colors show mid-mantle shear-velocity anomalies[51], radially averaged as annotated. As LLSVPs are primarily confined to 2,300-2,891 km depth[22,24], they do not dominate the radial average shown here. Note that the blue fast anomalies (downwelling conduits: "1","3"), are

$\sim 2\times$ weaker than the red slow anomalies (upwelling conduits: “2”,“4”) (Suppl. Figure S7). BEAMS likely occupy the volume between conduits (dashed outlines); arrows mark the sense of associated upper-mantle flow. Stagnant slabs[1] (“S”) should overlie BEAMS, guiding our assessment of BEAMS distributions, which well agree with cluster analysis of seismic-tomography models[25].

Figure 4 Illustration of the BEAMS hypothesis. BEAMS (light grey) are stable high-viscosity structures that reside in Earth’s lower mantle, while streaks of pyrolitic-harzburgitic rocks (light blue/green) and basalt (dark blue/green) circulate between the shallow and deep mantle through rheologically weak channels. BEAMS can coexist with, and stabilize the LLSVPs in the lowermost $\sim$500 km of the mantle (yellow), which are interpreted as intrinsically-dense (Fe-rich) piles[32,33,35] and plume-generation zones[31].

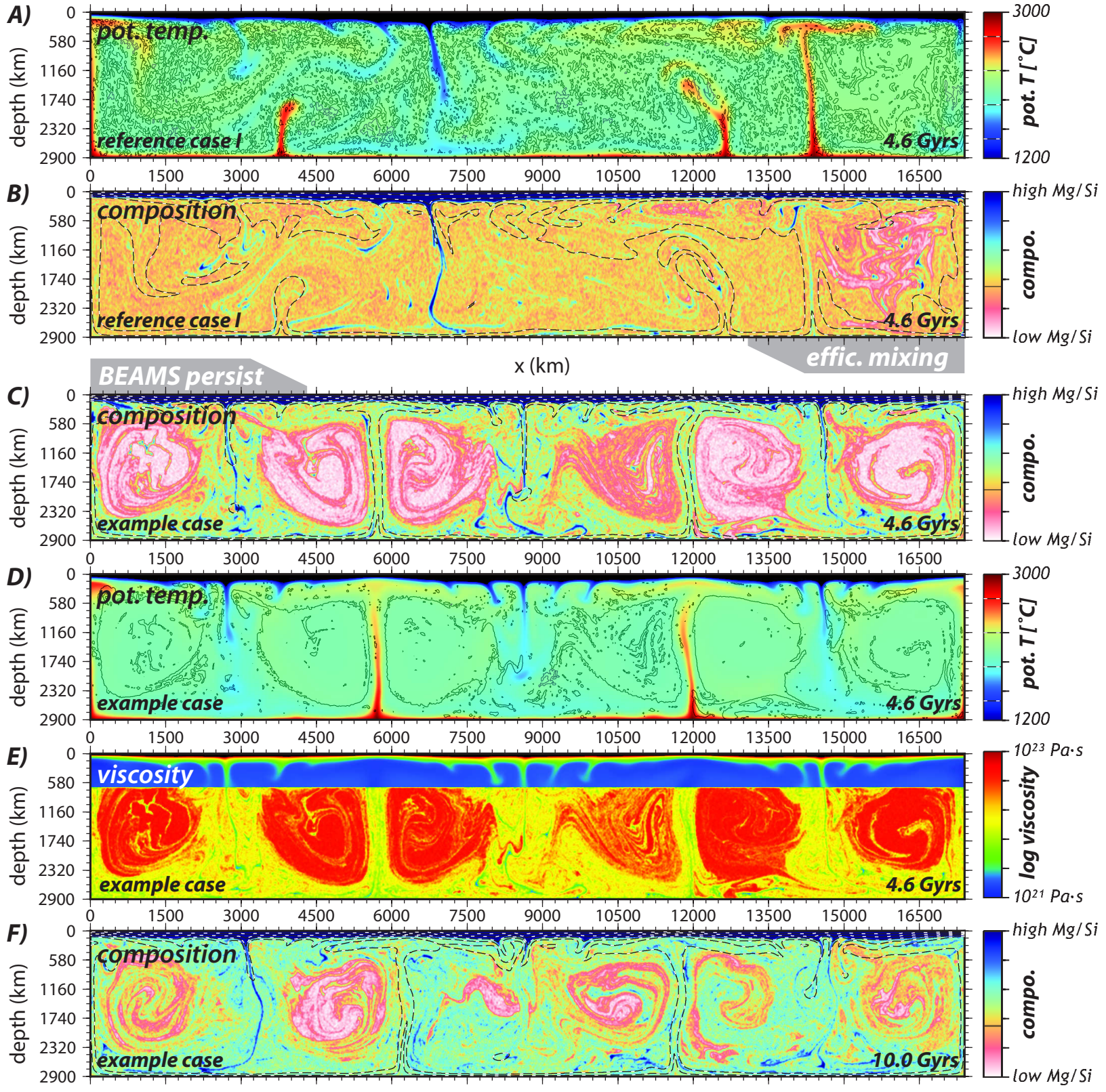
A)
pot. temp.
reference case I
4.6 Gyrs
3000
pot. T [°C]
1200
B)
composition
reference case I
4.6 Gyrs
high Mg/Si
compo.
low Mg/Si
BEAMS persist
effic. mixing
C)
composition
example case
4.6 Gyrs
high Mg/Si
compo.
low Mg/Si
D)
pot. temp.
example case
4.6 Gyrs
3000
pot. T [°C]
1200
E)
viscosity
example case
4.6 Gyrs
10²³ Pa·s
log viscosity
10²¹ Pa·s
F)
composition
example case
10.0 Gyrs
high Mg/Si
compo.
low Mg/Si
depth (km)
0
580
1160
1740
2320
2900
0
1500
3000
4500
6000
7500
9000
10500
12000
13500
15000
16500
x (km)

Figure 1

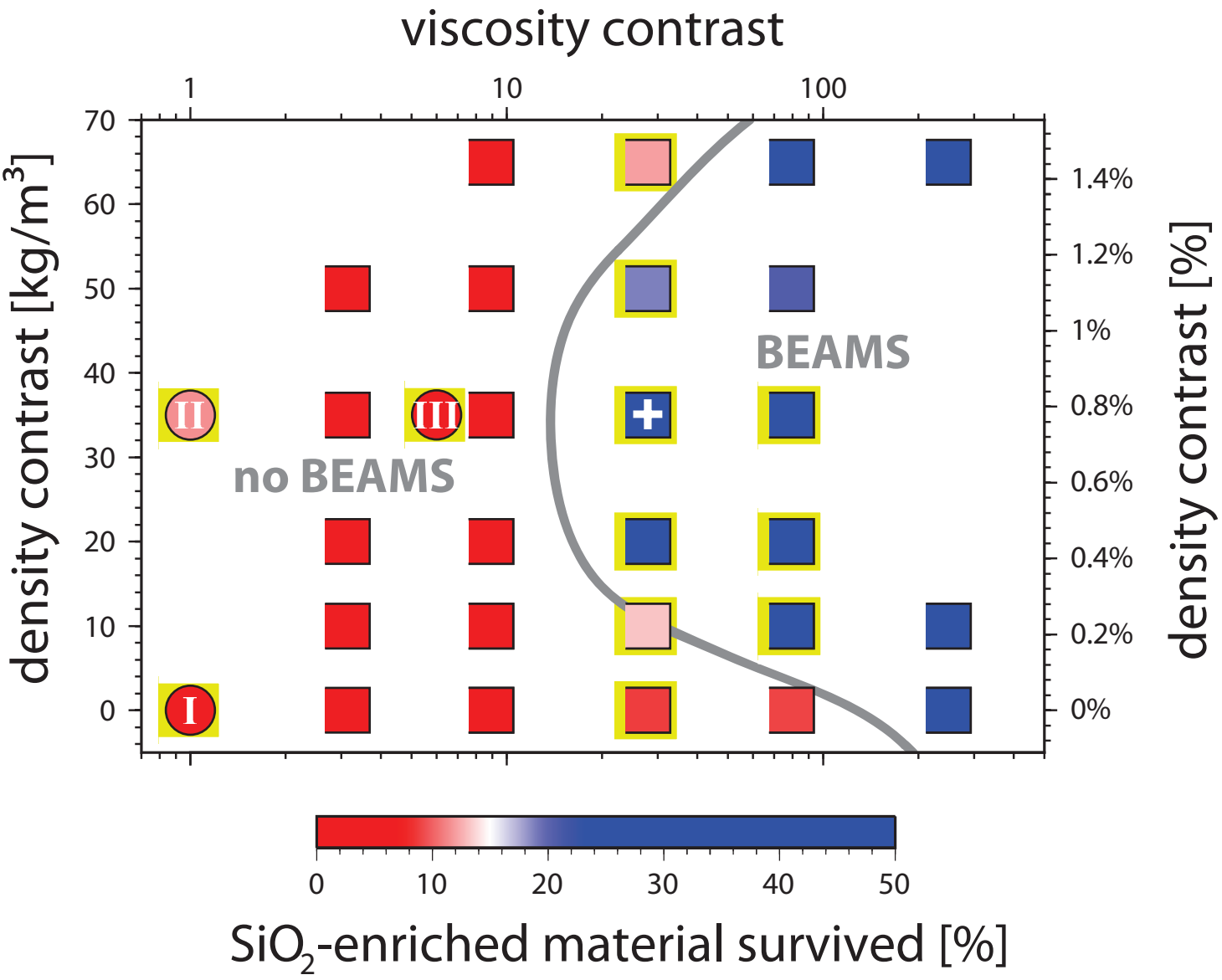
viscosity contrast
1
10
100
density contrast [kg/m3]
70
60
50
40
30
20
10
0
density contrast [%]
1.4%
1.2%
1%
0.8%
0.6%
0.4%
0.2%
0%
BEAMS
no BEAMS
I
II
III
0
10
20
30
40
50
SiO2-enriched material survived [%]

Figure 2

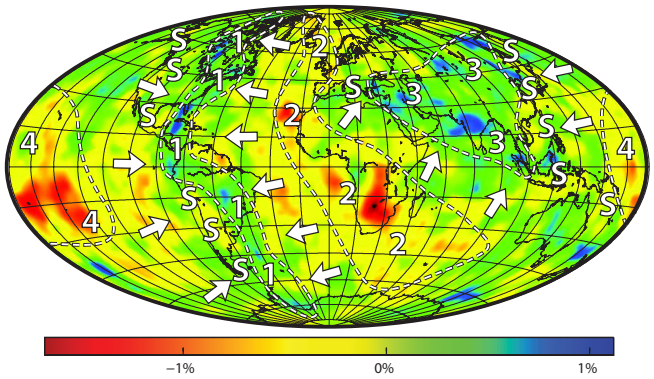

Lateral Shear Velocity Anomaly (1,000-2,200 km Depth Average)

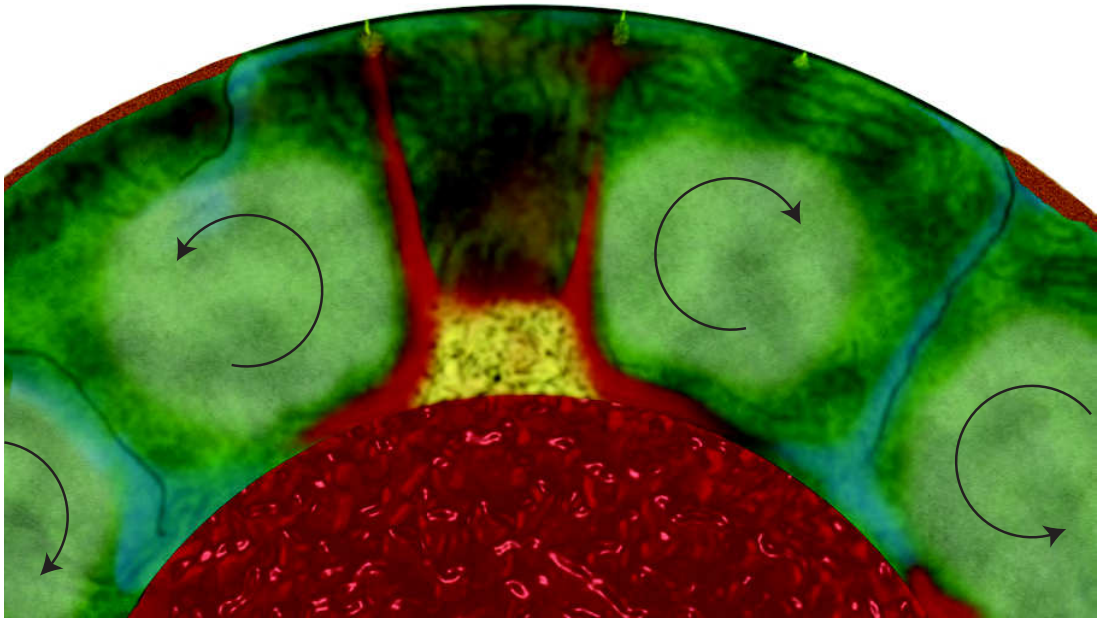

Figure 4